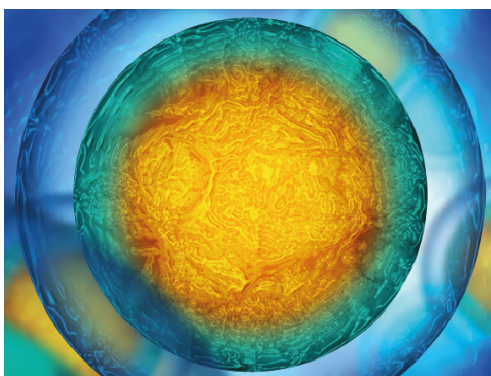


PAPER

Structural analysis across length scales of the scorpion pincer cuticle

To cite this article: Israel Kellersztein *et al* 2021 *Bioinspir. Biomim.* **16** 026013

View the [article online](#) for updates and enhancements.



Biophysical Society | **IOP | ebooks™**

Your publishing choice in all areas of biophysics research.

Start exploring the collection—download the first chapter of every title for free.

Bioinspiration & Biomimetics



PAPER

Structural analysis across length scales of the scorpion pincer cuticle

RECEIVED
11 October 2020

REVISED
19 November 2020

ACCEPTED FOR PUBLICATION
11 December 2020

PUBLISHED
27 January 2021

Israel Kellersztein^{*,1} , Israel Greenfeld¹  and H Daniel Wagner^{*} 

Department of Materials and Interfaces, Weizmann Institute of Science, Rehovot, 76100, Israel

* Authors to whom any correspondence should be addressed.

¹ These authors contributed equally to this work.

E-mail: israel.kellersztein@weizmann.ac.il and daniel.wagner@weizmann.ac.il

Keywords: hierarchical structures, arthropod exoskeleton, multiscale properties, laminate analysis, biological composites

Supplementary material for this article is available [online](#)

Abstract

Biological structures such as bone, nacre and exoskeletons are organized hierarchically, with the degree of isotropy correlating with the length-scale. In these structures, the basic components are nanofibers or nanoplatelets, which are strong and stiff but anisotropic, whereas at the macrolevel, isotropy is preferred because the direction and magnitude of loads is unpredictable. The structural features and mechanisms, which drive the transition from anisotropy to isotropy across length scales, raise fundamental questions and are therefore the subject of the current study. Focusing on the tibia (fixed finger) of the scorpion pincer, bending tests of cuticle samples confirm the macroscale isotropy of the strength, stiffness, and toughness. Imaging analysis of the cuticle reveals an intricate multilayer laminated structure, with varying chitin–protein fiber orientations, arranged in eight hierarchical levels. We show that the cuticle flexural stiffness is increased by the existence of a thick intermediate layer, not seen before in the claws of crustaceans. Using laminate analysis to model the cuticle structure, we were able to correlate the nanostructure to the macro-mechanical properties, uncovering shear enhancing mechanisms at different length scales. These mechanisms, together with the hierarchical structure, are essential for achieving macro-scale isotropy. Interlaminar failure (ILF) analysis of the cuticle leads to an estimation of the protein matrix shear strength, previously not measured. A similar structural approach can be adopted to the design of future synthetic composites with balanced strength, stiffness, toughness, and isotropy.

1. Introduction

Scorpions are predatory arachnids from the phylum of arthropods having a pair of chelae (pincers) that vary in shape and size among different scorpion species [1]. The chela consists of two different segments: (i) the tarsus, which is the movable finger, and (ii) the tibia, which is the fixed finger and the base of the chela (figures 1(a) and (b)) [2]. The scorpion uses its multifunctional chela for prey handling, defense, or mating, each inducing different mechanical stresses in the exoskeleton.

In contrast to the extensive research done on the exoskeleton of crustaceans such as crabs and lobsters [3–6], the scorpion chela microscale composition, and particularly its hierarchical structure, are largely unexplored [7–10]. Moreover, mechanical

calculations have ignored the chela multiscale properties [1, 11], and its functionality was addressed by considering the biological tissue as a single homogeneous structural unit [11, 12]. These knowledge gaps, particularly in the correlation between the chela cuticle microstructure and its macro-mechanical properties, are due to the limited and dated structural investigations and scarce studies simulating the mechanical properties from bottom-up. To bridge the gaps, the present study offers an in-depth investigation of the chela exoskeleton of the *Scorpio Palmatus* (SP), which considers its multiscale structure and related effects on the mechanical properties. Specifically, the cuticle of the tibia base, referred to as tibia throughout the text, is the focus of this study.

Structural analysis of the SP tibia cuticle revealed the existence of an intermediate layer. This layer is

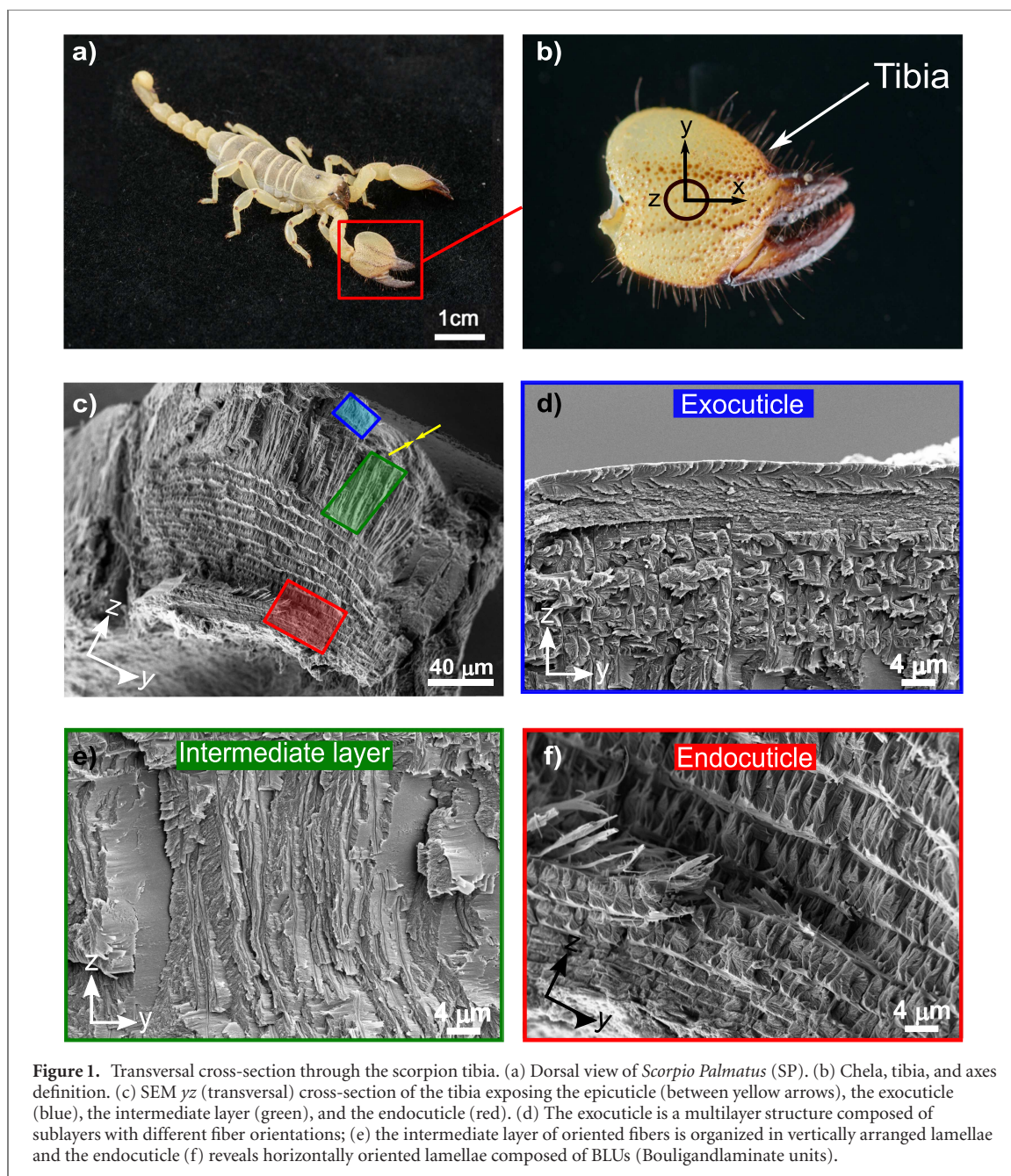


Figure 1. Transversal cross-section through the scorpion tibia. (a) Dorsal view of *Scorpio Palmatus* (SP). (b) Chela, tibia, and axes definition. (c) SEM yz (transversal) cross-section of the tibia exposing the epicuticle (between yellow arrows), the exocuticle (blue), the intermediate layer (green), and the endocuticle (red). (d) The exocuticle is a multilayer structure composed of sublayers with different fiber orientations; (e) the intermediate layer of oriented fibers is organized in vertically arranged lamellae and the endocuticle (f) reveals horizontally oriented lamellae composed of BLUs (Bouligandlaminat units).

made of stacked lamellae reinforced by chitin fibers, absent in the cuticle of arthropods having claws [4]. The presence of such layer was previously found by Mutvei [10] in the tarsus of the *Heterometrus Spinifer*, and further studied at the microscale by Kellersztein *et al* [13] in the tarsus of the SP, both species of scorpions belonging to the biological class of arachnids. Here, we present evidence of such a layer in the tibia of the SP, which increases the local thickness of the tibia cuticle, and as will be seen, has a significant impact on the mechanical properties of the cuticle assembly. Combining an experimental methodology with theoretical analysis, we show how this layer affects the cuticle structure under different hydration conditions. An attempt is made to address the question why it evolved in the scorpion tibia.

In this study, high-resolution scanning electron microscopy (SEM), transmission electron microscopy (TEM) and atomic force microscope (AFM) images of the scorpion tibia cuticle reveal the microstructural details of the biological tissue, focusing on the intermediate layer. Bending tests under dry and wet conditions measure the stiffness, strength, and work to fracture properties of the tibia cuticle, demonstrating high degree of in-plane isotropy. Classical laminate analysis, taking into account the cuticle ~ 40 layers, correlates the observed microstructure with the measured macro-mechanical properties, exposing hidden structural features such as shear interlocking between helical sub-structures (Bouligands) and fibrous interconnections between chitin fibers in a lamina. We further show how macrolevel

isotropy is built up by the proper organization of the anisotropic nanocomponents across the structural length scales. The analysis captures the mechanical significance of the intermediate layer on the functionality of the scorpion chela, and simulates variations in the intermediate layer thickness and angular direction, towards possible scientific and engineering implementations.

2. Materials and methods

2.1. Scorpions collection and handling

Adult animals from the species SP (figure 1(a)) were collected with authorization from the Israel Nature and Parks Authority and in collaboration with The Hoopoe Yeruham's Ornithology and Ecology Center of Israel. The collection took place in the Negev desert in the area of Sde Boker, in the south of Israel. During transportation, the scorpions were separately kept in plastic containers sealed inside a hard-plastic box with the aim of preventing escape during transportation. The scorpions were euthanized by submerging them in liquid nitrogen and subsequently stored in plastic bags inside carton boxes in a freezer at -80°C . The euthanizing method used in this research is well supported in the literature as humane while preserving the integrity of the exoskeleton structure [13–16]. The chelae were manually separated from the rest of the scorpion body using a razor blade, before experimentation.

2.2. Scanning electron microscopy (SEM)

The preparation process for the structural analysis of the chelae samples began with fixing overnight the biological tissue at 4°C in a fixation buffer containing 2% glutaraldehyde and 3% paraformaldehyde in 0.1 M cacodylate buffer (pH 7.3). Subsequently, the samples were submerged for three additional days in a new fixation buffer at 4°C . Three rinses of 10 min each with 0.1 M cacodylate, were employed to remove any excess of aldehyde from the fixation process. To produce an enhanced image contrast in the electron microscope, samples were post-fixed in 1% OsO_4 in 0.1 M cacodylate buffer at room temperature for 1 h. Samples were cleaned over in 0.1 M cacodylate buffer and held in a critical point drying machine sample holder, and dehydration was reached using graded ethanol concentrations of 30%, 50%, 75%, 90%, and 100%. Lastly, samples were placed in a critical point dehydration (CPD) machine (baltec CPD 030). Transversal cross-sectional samples were prepared from the tibia exoskeleton by manually breaking the tissue.

High-resolution scanning electron microscopy (HRSEM) images were obtained using a Sigma 500 (Zeiss, Oberkochen, Germany). Images were obtained using a secondary electron (SE2) detector at a working distance of 14–15 mm, to reach an improved field of view, and an acceleration voltage of 5 kV. Samples

for structural characterization of the tibia were coated with a gold–palladium alloy before SEM imaging, using an Edwards (Sanborn, NY) S150 sputter coater. Surface fractures from bending samples were covered with a 6.5 nm layer of iridium before SEM imaging, using a Safematic coater instrument. All dimensional measurements were performed using ImageJ software. SEM images from the tibia of three different animals were obtained for the structural analysis.

2.3. Transmission electron microscopy (TEM)

The sample preparation process was similar to that for SEM. Following fixation with 1% OsO_4 the samples were washed and then conserved with 2% uranyl acetate (UA) for an hour at room temperature. Then, samples were dehydrated in graded ethanol series, and rinsed with acetone twice before embedding in epoxy resin (Epon, Embed 812, EMS, USA). The samples were incubated in 30% epoxy resin diluted in acetone solution overnight at room temperature and then 4 h in 50% epoxy resin. Lastly, the samples were moved to a 70% epoxy resin solution overnight, followed by incubation in 100% epoxy resin for 4 h, then overnight and finally for 2 h in 100% resin. Final samples embedded in epoxy resin were placed in silicon molds, and the polymerization process was carried out over three days in an oven heated to 60°C .

An Ultracut UCT microtome (Leica) was used to obtain thin slices (~ 100 nm) of the embedded tibia, further stained with 2% uranyl acetate and Reynold's lead citrate and then examined using FEI Tecnai T12 TEM operating at 120 kV. Images were recorded with a bottom-mounted $2\text{k} \times 2\text{k}$ Eagle CCD camera (FEI, Eindhoven). All dimensional measurements were performed using ImageJ software.

2.4. Atomic force microscopy (AFM)

The tibia was initially dehydrated in ethanol and then embedded in a three-component epoxy resin. The embedded tibia sample was subsequently polished down to 4000 grit SiC papers, followed by polishing the exposed surface with polycrystalline diamond suspensions (Struers) having a particle size of $1\ \mu\text{m}$. AFM imaging was carried out using a custom AFM system, a combination of the Smart AFM and OmegaScope (Horiba). Scans were made in contact mode, using silicon on nitride lever probe (Bruker SNL-B) with a spring constant of $0.12\ \text{N m}^{-1}$.

2.5. Bending test

Rectangular shaped samples ($5\text{L} \times 1.1\text{W} \times 0.12\text{T mm}^3$) were manually cut from the SP tibia of at least three scorpions using a home-made sample cutter with a controlled spacer. The specimens were oriented with respect to the chela long axis (figure 1(b)), where the x -axis is parallel to the chela long axis (0°), and the y -axis is the orthogonal orientation (90°). A set of samples (i.e. samples from all orientations) was dehydrated in gradual series of

ethanol, consisting of two rinses of 15 min each at 30%, 50%, 75%, and 90% concentration, and two additional rinses of 30 min each at 100% concentration, to remove the excess of water. A second set of samples for each orientation was immersed in deionized water; hydrated samples achieved maximum weight after 48 h.

Quasi-static three-point bending tests were carried out using a Discovery DMA-850 instrument with an open oven. The test span was 4.1 mm, resulting in a specimen span length to thickness ratio of approximately 35. A preload force of 0.03 N was applied, and the loading rate was 0.3 mm min⁻¹ using a rate control-strain ramp condition. The overall specimen thickness was measured from SEM images using the ImageJ software. From each load-displacement curve, the flexural modulus E_f (MPa), stiffness K_f (N mm²), and strength σ_f (MPa) were calculated using the following formulae:

$$E_f = \frac{m}{4w} \left(\frac{l}{t} \right)^3 \quad (1)$$

$$K_f = E_f I = \frac{m}{48} l^3 \quad (2)$$

$$\sigma_f = \frac{3Pl}{2wt^2}, \quad (3)$$

where m (N mm⁻¹) is the slope in the elastic region of the force-displacement curve, P (N) is the applied load, l (mm) is the span length, w (mm) is the specimen width, and t (mm) is the specimen height (equal to the cuticle thickness). The flexural modulus and strength represent the properties of a beam that has the same dimensions and load-displacement curve as the tested specimen, where the beam is homogenous and isotropic. In other words, for a uniform isotropic beam, the flexural modulus and strength are roughly comparable to the tensile modulus and strength, respectively. The flexural stiffness represents the actual bending stiffness of the beam (force/deflection or moment/curvature).

3. Results and discussion

3.1. Cuticle multilevel microstructure

SEM images from a transversal cross-section (yz) of the SP tibia expose a multilayered structure within the exoskeleton. The different layers—four in total—are distinguishable according to their fiber arrangement and morphology (top-down in the z direction): the epicuticle, the exocuticle, an intermediate layer, and the endocuticle [figures 1(c) and S1 (<https://stacks.iop.org/BB/16/026013/mmedia>)]. The multilayer design displays a similar structural arrangement as in the SP tarsus [13].

The epicuticle is the outermost layer (indicated by yellow arrows in figure 1(c)) and is the thinnest in the tibia exoskeleton—several hundreds of nm. The next layer, below the epicuticle, is the exocuticle (figure 1(d)), a structural layer ~ 20 μm thick

further divided into four sublayers of different fiber orientations. The layer at the exocuticle top is an anisotropic layer of fibers oriented at an angle close to the x -direction; then, an in-plane isotropic layer made of platelets parallel to the xy plane; next, a second anisotropic layer of fibers oriented in the x -direction; and finally, a layer made of horizontally oriented (parallel to the xy plane) multilayers composed of Bouligand laminate units (BLUs). A BLU is a helical stack of unidirectional fibrous layers, located one upon the other completing a 180° rotation [16].

A ~ 37 μm thick intermediate layer made of unidirectional fibers oriented in the x -direction and arranged in vertical lamellae is uncovered below the exocuticle (figure 1(e)). The fibers in this layer seem longer than the discontinuous fibers observed in the tarsus intermediate layer, reported in Mutvei [10] and Kellersztein *et al* [13]. The intermediate layer constitutes $\sim 30\%$ of the total tibia cuticle thickness. The innermost layer is the endocuticle (figure 1(f)), a horizontally oriented multilayer structure identified by the presence of Bouligand units; the endocuticle has an overall thickness of ~ 64 μm . As in the SP tarsus, the BLUs in the tibia possess particular features not reported in other arthropod exoskeletons such as in the mantis shrimp or lobsters [8, 9]; these features, which are described in [16] and pointed in figure S1(c), are: (i) off-axis twisting and out-of-plane tilting of the different laminae in the BLU, (ii) separation of the BLU layers by a thicker interlayer, and (iii) separation of the BLUs by a thinner intralayer.

An additional structural feature is observed in the tibia surface, where the tissue is not entirely flat (figures 2(a) and S2(a)). The presence of irregularities in the tibia cuticle external plane—resembling ‘mountains’—affects the local thickness of the tibia cuticle, spanning from 97 μm at the thinnest areas (planar areas) up to 147 μm at the highest point in such mountains (figure S2(b)), resulting in an average cuticle thickness of ~ 120 μm (table 1). It was further perceived that due to the presence of such ‘mountains’, the internal structure of the tibia exoskeleton is not uniform. The intermediate layer (figures 1(c) and (e)) is only present in the thicker regions of the tibia cuticle, where such ‘mountains’ appear (figures 2(b) and (d)). In contrast, a uniform horizontal lamellae structure composed of the other three layers was observed in the ‘flat’ sections (figure 2(c)), as seen in the AFM images in figure 2. It can also be observed that the intermediate layer has a thickness gradient in the xy plane, e.g. the intermediate layer region displayed in figure 2(d) is thicker than the one exposed in figure 2(b) (see representative profiles in figure S3). The question arises why the intermediate layer is housed in an array of ‘mountains’ rather than in a layer having constant thickness; there is most likely a biological reason behind this conformation, but its investigation is not within the scope of the current research.

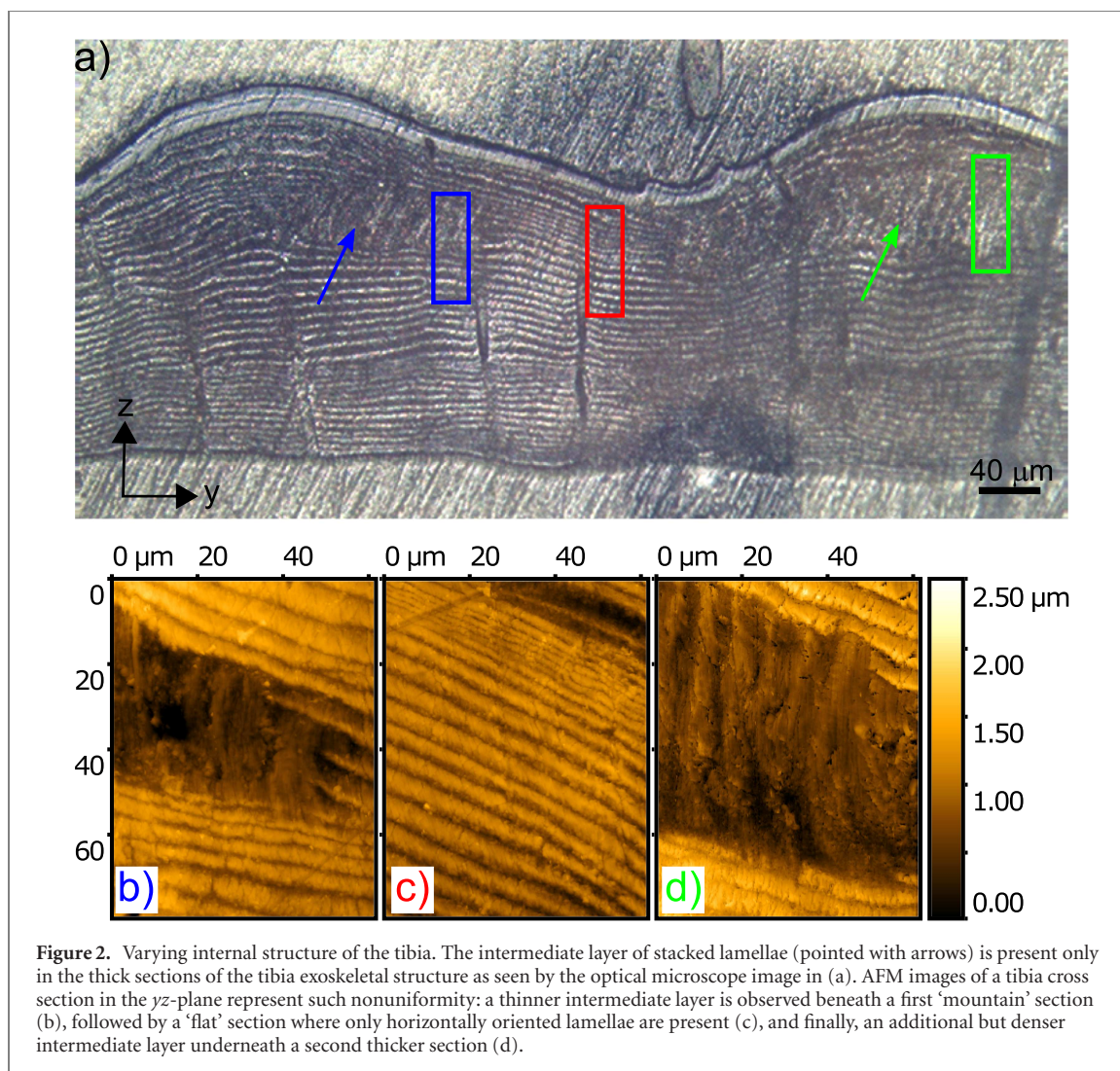


Figure 2. Varying internal structure of the tibia. The intermediate layer of stacked lamellae (pointed with arrows) is present only in the thick sections of the tibia exoskeletal structure as seen by the optical microscope image in (a). AFM images of a tibia cross section in the yz -plane represent such nonuniformity: a thinner intermediate layer is observed beneath a first ‘mountain’ section (b), followed by a ‘flat’ section where only horizontally oriented lamellae are present (c), and finally, an additional but denser intermediate layer underneath a second thicker section (d).

Table 1. Mechanical properties of the SP tibia (mean values and standard deviation).

Sample orientation (°)	Number of samples tested		Thickness (μm)		E_f (GPa)		σ_f (MPa)		W_f (mJ mm ⁻²)			
	Dry	Wet	Dry	Wet	Dry	Wet	Dry	Wet	Elastic		Plastic	
									Dry	Wet	Dry	Wet
0	7	5	117 ± 2	112 ± 7	11.1 ± 2.3	4.1 ± 1.1	270 ± 33	102 ± 24	0.6 ± 0.3	0.2 ± 0.2	1.1 ± 0.7	0.9 ± 0.4
45	9	6	120 ± 1	123 ± 9	9.1 ± 3.3	3.7 ± 1.0	235 ± 58	126 ± 30	0.8 ± 0.2	0.4 ± 0.2	0.7 ± 0.4	1.1 ± 0.4
90	12	7	122 ± 1	112 ± 9	7.3 ± 2.0	4.9 ± 1.7	210 ± 63	135 ± 72	0.8 ± 0.4	0.3 ± 0.3	0.7 ± 0.4	1.1 ± 0.7

The tibia cuticle is a multilevel, multiscale, hierarchical, laminated structure consisting of eight levels [13, 16]: (1, 2) N-acetyl-glucosamine sugar molecules are polymerized into crystalline α -chitin chains, (3) which are packed in ~ 5 nm chitin-protein fibrils. These chitin-protein nanofibrils are the basic composite component of the tibia exoskeleton. (4) The fibrils are collected into 50–100 nm fibers, which are next (5) compactly packed into unidirectional laminae of xy dimensions $\sim 2 \times 2 \mu\text{m}^2$. At this level of hierarchy, the chitin protein laminae are assembled into multiple layers as in the intermediate layer (6), or packed in platelets to form the second sub-

layer in the exocuticle (6), or assembled into a Bouligand unit (40–100 laminae), each at a specific orientation (6). The Bouligand units (length \times width $\sim 2 \times 2 \mu\text{m}^2$, typical total height 4–6 μm) are assembled in a 2D array into a Bouligands layer, with separating intralayers (100–200 nm thick); (7) Bouligand layers are assembled one on top of each other, with separating interlayers (1–2 μm thick), a total of ~ 5 layers in the exocuticle and ~ 14 layers in the (7) endocuticle; The exocuticle (7) is made of the Bouligands stack, the two unidirectional laminae, and the platelets lamina; (8) the cuticle is an assembly of the 4 major layers that form the entire chela exoskeleton.

3.2. Bending stiffness and strength

Bending tests were conducted to measure the mechanical behavior of the SP tibia exoskeleton in three directions. The relevant properties (bending modulus (E_f), strength (σ_f) and work to fracture (W_f) are detailed in table 1. The dry and wet mechanical properties of the cuticle provided in table 1 represent the two extreme boundaries for the cuticle degree of hydration, and therefore the cuticle's mechanical properties in the natural state (*in vivo*) are expected to reside between these boundaries. Comparison of the data exposed in table 1 to the cuticle of other species of scorpions is not possible as such data has not been reported in the literature.

The flexural force-displacement curves show that all specimens display an initial linear elastic response followed by an inelastic response (figures 3(a) and (b)). After reaching the maximum stress, most of the dehydrated samples failed catastrophically, whereas in some samples failure occurred progressively (figure 3(a)). In the case of hydrated specimens (figure 3(b)), a higher scattering of the force-displacement curves is observed together with longer displacements. These samples maintain a relatively constant maximum force plateau, displaying a characteristic damage tolerance behavior [17]. In the plateau region (figure 3(b)), a fluctuation of the force is seen, likely the result of gradual breaking of the different layers inside the cuticle, reflecting a typical failure behavior of laminated composite materials [18]. For most hydrated specimens, fracture was never reached.

The force-displacement curves also demonstrate that an increase in the water content within the tibia, simultaneously reduces the bending modulus (E_f) and strength (σ_f) of the biological composite, as seen in figures 3(c) and (d). The decrease is a consequence of the presence of hydroxyl groups ($-OH$) within the chitin molecules. In the vicinity of water, such OH groups form hydrogen bonds with the water molecules instead of bonding with adjacent chitin molecules; then, the water-chitin bonding leads to an enlargement of the free volume between chitin fibers, resulting in degradation of the mechanical properties of the tibia exoskeleton [19, 20].

We observe that the sample orientation has a relatively small impact on the bending properties of the cuticle. As the majority of the chitin fibers within the tibia exoskeleton are oriented parallel to the x -axis, it might be expected to see much higher bending modulus and strength values for the 0° samples in figures 3(c) and (d), respectively. Although the tibia is made of anisotropic components (i.e. α -chitin and proteins) and layers (e.g. the intermediate layer of oriented fibers), at the macro scale the mechanical properties display a quasi in-plane isotropic behavior. This outcome results from the hierarchical structure of the tibia, in which the many anisotropic laminae are arranged and oriented differently at each level; when

the structure functions as a single unit under external stresses such as bending, the anisotropic effect of the components and the layers is weakened [21]. This finding is corroborated by the laminate analysis described further on.

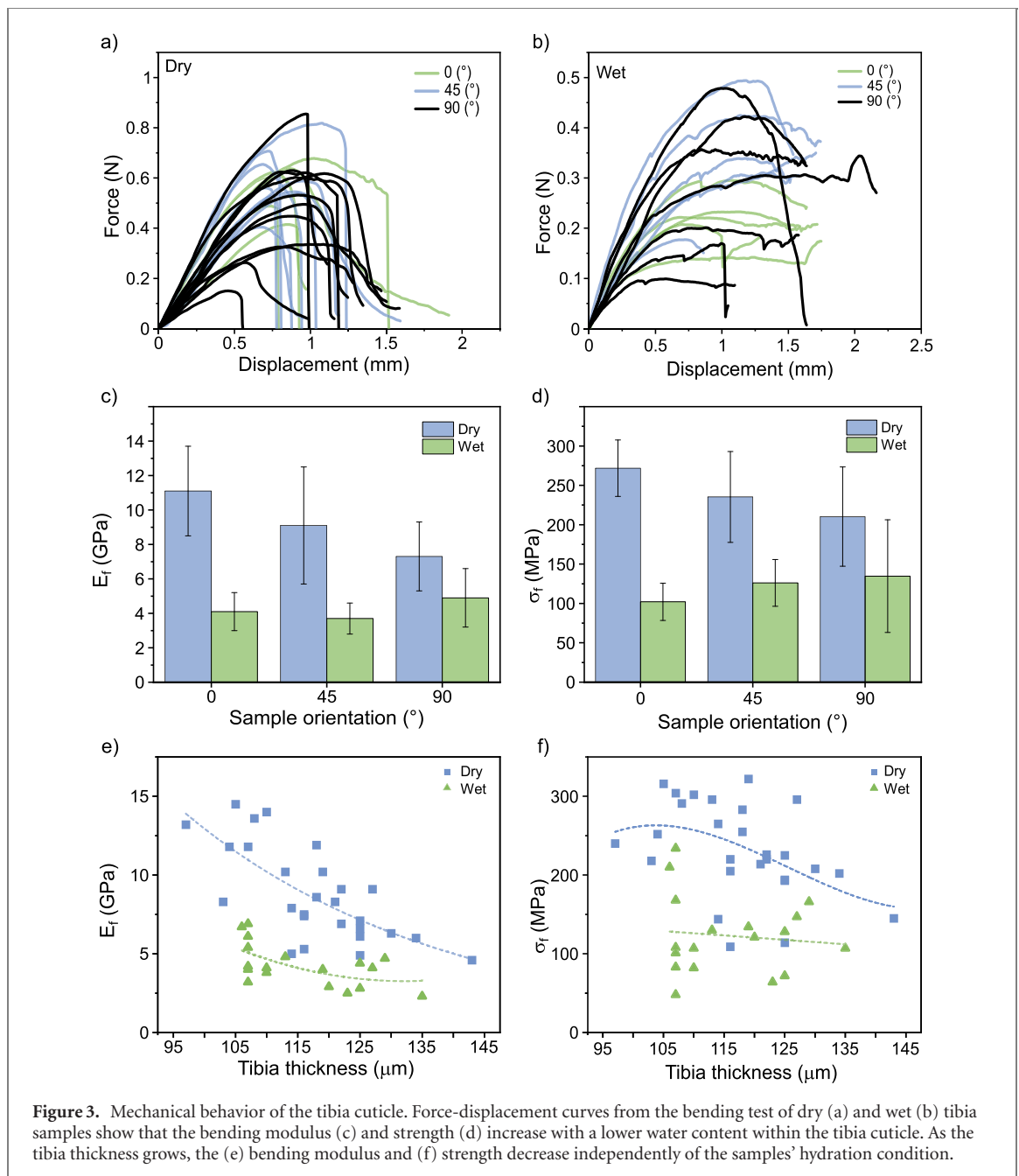
Analysis of E_f and σ_f versus the tibia thickness provides further insights about the presence of the intermediate layer. Both the bending modulus and strength decrease as the tibia thickness increases (figures 3(e) and (f)). However, the bending strength for the hydrated samples seems less sensitive to the tibia thickness. The data suggest that at the higher levels of hierarchy, the mechanical properties of the tibia are mainly dictated by the structural assembly formed within the cuticle rather than by the properties of the materials that compose the cuticle. In other words, the arrangement of the cuticle laminate with an added intermediate layer modifies the structural hierarchy, with the result of decreasing its mean flexural modulus and strength. However, although the use of material in this structure is thus less efficient for flexural loading, the overall structural performance under given external loads improves as a result of a higher moment of inertia of a thicker tibia. This is clearly seen in the increase of the bending stiffness (force/deflection or moment/curvature) with increasing tibia thickness (figure S4), and similarly for the strength.

3.3. Toughness

Most tibia exoskeleton samples are still capable of carrying load beyond the peak stress, regardless of the fracture mode, as seen in figures 3(a) and (b). This is remarkable when compared with synthetic brittle fiber-reinforced polymeric materials that possess similar bending modulus and strength [22, 23], which did not exhibit load carrying beyond the peak stress. Thus, the multiscale arrangement of materials is responsible for the balancing of the flexural stiffness, strength, toughness and in-plane isotropy of the tibia cuticle. To achieve such balance, the cuticle implements a trade-off between hard and soft components (chitin fibers and protein matrix) together with multilayered hierarchical laminate arrangement (i.e. laminae ordering and orientation).

To provide evidence of such toughening capacities, we quantified the energy required to fracture the biological tissue in terms of work to fracture (figure 4(a)). As for the bending modulus and strength, the total work to fracture of the tibia follows a nearly in-plane isotropic behavior in all specimens and hydration conditions (a slight difference was observed in the 0° oriented samples). These results are significant, considering other biological structures where the presence of water leads to a deterioration of the work to fracture [24].

A dehydrated tibia cuticle can absorb higher quantities of energy in the elastic regime. By contrast, a hydrated cuticle uses its inelastic behavior to



increase the toughness of the structure, as suggested in figure 4(a). This difference in energy dissipation is demonstrated in figure 4(b), where yielding is reached at higher forces and displacements in a dry cuticle compared to the wet cuticle, which absorbs higher amounts of energy through longer plastic deformation.

Different failure mechanisms enhance the energy required to fracture a biological tissue [16] according to the hydration conditions of the tibia. Figure 4(c) shows the lateral cross-section of a representative dry tibia cuticle sample after three-point bending, where delamination seems imminent as the primary mode of failure, while first ply failure (FPF) can take place as well. Delamination failure occurs when the shear stresses between adjacent laminae exceed the inter-laminar bonding strength, in the present case, that

of the proteinaceous matrix. A FPF occurs when the in-plane laminate stresses exceed the strength of the highest stressed lamina, consisting here of unidirectional chitin fibers embedded in a proteinaceous matrix.

Delamination failure is likely the result of high anisotropy in fracture resistance with respect to the fiber orientation within the structure [25]. In the case of the tibia cuticle, this happens at the cuticle thicker sections as a result of the higher stiffness and anisotropic nature of the intermediate layer. This is evidenced by the wider crack seen in the thicker areas of the cuticle in figure 4(c), implying that the crack initiates where the intermediate layer is present and the structure is stiffer (see figure S4): a thinner crack runs symmetrically from both sides of the 'mountain'

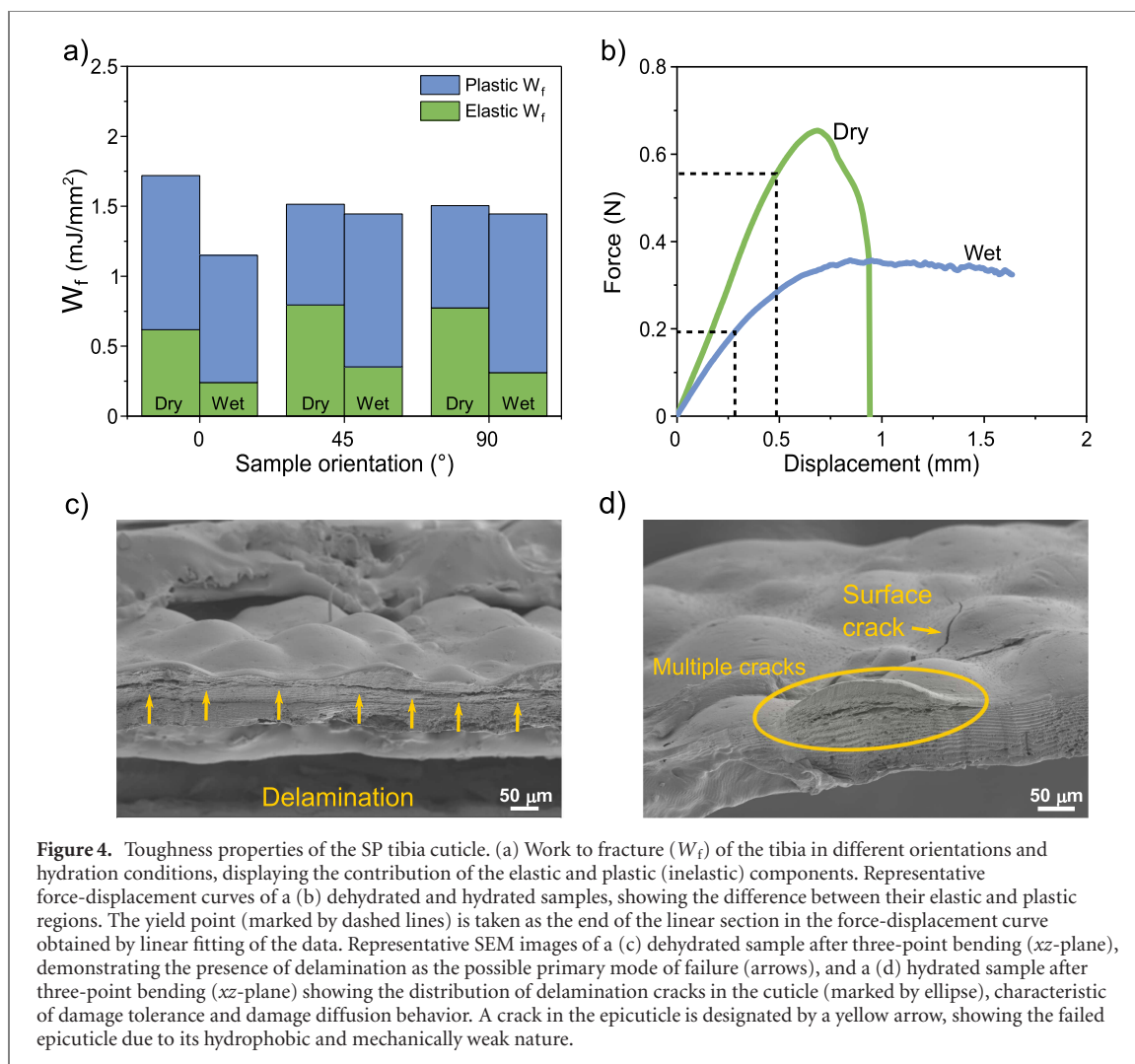


Figure 4. Toughness properties of the SP tibia cuticle. (a) Work to fracture (W_f) of the tibia in different orientations and hydration conditions, displaying the contribution of the elastic and plastic (inelastic) components. Representative force-displacement curves of a (b) dehydrated and hydrated samples, showing the difference between their elastic and plastic regions. The yield point (marked by dashed lines) is taken as the end of the linear section in the force-displacement curve obtained by linear fitting of the data. Representative SEM images of a (c) dehydrated sample after three-point bending (xz -plane), demonstrating the presence of delamination as the possible primary mode of failure (arrows), and a (d) hydrated sample after three-point bending (xz -plane) showing the distribution of delamination cracks in the cuticle (marked by ellipse), characteristic of damage tolerance and damage diffusion behavior. A crack in the epicuticle is designated by a yellow arrow, showing the failed epicuticle due to its hydrophobic and mechanically weak nature.

towards the flat areas. This finding is supported by the strength analysis described further on.

A similar sample but of wet tibia after three-point bending is presented in figure 4(d). Two main features are visible concerning the failure of the tibia: (i) cuticle surface failure (see the yellow arrow in figure 4(d)) and (ii) damage tolerance (multiple breaks, see the yellow ellipse in figure 4(d)). Some surface cracking was apparent in the wet tibia sample, which corresponds to failure of the epicuticle. The epicuticle is the only layer that does not contain chitin fibers, therefore, it is relatively weak and its mechanical contribution to the overall mechanical properties of the exoskeleton is insignificant [13]. The epicuticle is a homogeneous layer made of hydrocarbons [7, 13, 26], which are responsible for the hydrophobic nature of this layer. Thus, the tibia structure has two different hygroscopic states, such that the epicuticle repels water and remains brittle, whereas the other layers soak water and become more ductile. Under stress, which is highest at the surface of a bent beam, the epicuticle collapses because of both its brittleness and weak strength. By contrast, the other layers are capable of resisting stresses for longer deformations.

The force-displacement curves in figures 3(b) and 4(b) show that although the structure is failing plastically, the tibia can still carry stresses for long displacements. This is the consequence of gradual breaking of the layers, known as damage tolerance [17], evidenced in the tiny steps seen in the wet curve, each reflecting the failure of a single layer or interface. Also, the tibia cuticle exhibits areas with characteristic diffused damage, where the cracks are randomly distributed across the structure thickness (figure 4(d)) rather than running along the tibia beam as a localized delamination. These two toughening mechanisms, damage tolerance and diffused damage, lead to improved energy absorption of the plastic region in the wet tibia structure. Additional toughening mechanisms such as fiber-matrix interface debonding and fiber bridging are also seen in the tibia fractures (figure S5) [27].

3.4. Laminate elastic modeling

The tibia cuticle structure is a multilayer laminate made of three major layers, the exocuticle, the intermediate layer, and the endocuticle, each layer hierarchically assembled and optimized into a singular structural unit which can bear external stresses,

eventually beneficial for the survivability of the scorpion (figure 5(a)). The tibia laminate is capable of accommodating different types of stresses, for the attack and defense functionality of the animal, and, at the same time, to fit biological purposes such as protecting the animal from the environment or during mating [2, 12]. The direction of these external stresses cannot be predicted, and therefore mechanical uniformity is important: the endo- and the exocuticle are both nearly in-plane isotropic layers, that is their properties are similar within the xy plane, whereas the intermediate layer is anisotropic because its fibers are unidirectional [13].

Based on experimental observations, the tibia exoskeleton can be viewed as a fiber-reinforced composite material, structurally built as thin multilayer laminate. The individual layers comprising the laminate, about 40 in total, are all parallel to the xy plane but their fibers are oriented in different directions in each layer (in-plane). In general, a laminate excels in bearing in-plane stresses, which can be induced by in-plane tension as well as by out-of-plane bending, the latter being the focus here.

Theoretical analysis of such an intricate laminate is significant for understanding the biological motivation behind this structure, and the potential benefits that can be learnt from it when designing structural bioinspired composites. A central issue to be addressed is the role of the anisotropic layer between the two nearly isotropic layers, and its effect on the mechanical functionality of the scorpion tibia. No less important, the impact that the presence of such a layer may have in future synthetic structural materials.

To this end, classical laminate theory (CLT) [18] was used. CLT has been applied in the past to analyze the mechanical properties of other arthropod cuticles [4, 16]. This approach seems suitable to model the mechanical properties of the tibia exoskeleton, considering that the cuticle laminate is neither symmetric nor balanced, and therefore its mechanical behavior is difficult to predict. A symmetric lamina consists of pairs of identical laminae of equal orientation and at equal distances from the midplane. A balanced lamina consists of pairs with orientations of opposite signs, thus not symmetrical with respect to the midplane. Both requirements are not upheld in the cuticle laminate. Stress coupling effects are thus likely to appear in the cuticle, resulting in intricate combinations of extensional, flexural, and torsional deformations.

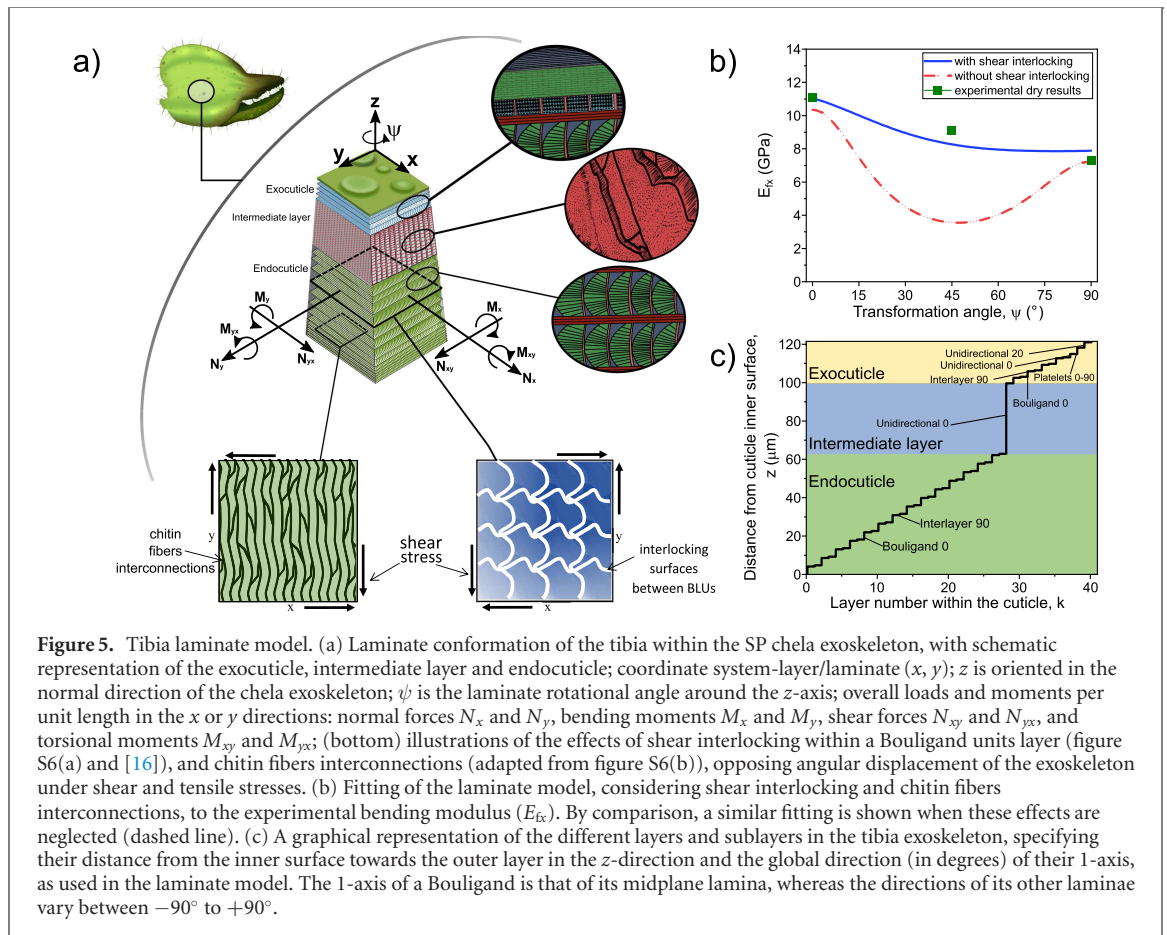
This analysis was performed for the 42 layers that compose the tibia laminate, as geometrically modeled in figure 5(c). The tibia laminate satisfies the laminate analysis fundamental assumptions [18, 28]: (i) each layer (lamina) is quasi-homogeneous and orthotropic, so that its structure and elastic properties are uniform in each of the orthogonal directions x, y, z , although different in every direction; (ii) the laminate has high aspect ratio (length/thickness), so

that its layers may be considered to be in a plane-stress state; and (iii) the elastic displacements under load are small compared to the cuticle thickness. The tight packing of the tibia laminate observed in figures 1(c)–(f) and illustrated in figure 5(a) (no gaps are visible between the different structural elements) guarantees efficient stress transfer between layers, and therefore the laminate is essentially in a plane-stress state as assumed. Some modelling assumptions and adaptations are needed for the Bouligand layers in the exo- and endocuticle, as for the platelets layer in the exocuticle, as now described.

A first assumption is to consider each Bouligand layer in the endo- and exocuticle as a single orthotropic layer, which reflects the elastic properties of the Bouligand's entire internal multilayer structure. The mechanical properties of a Bouligand unit in the tarsus of the SP were previously calculated by Greenfeld *et al* [16], and are adapted here. A second assumption is related to the presence of a platelet-like layer in the exocuticle. Laminate analysis assumes that all plies are composed of orthotropic layers, characteristically of fiber-reinforced laminae. To simplify the analysis, we considered the platelets ply as a randomly oriented fibers layer. Although from figures 1(e) and S1(b) one can appreciate that the fibers within the intermediate layer have a certain degree of orientation with respect to the x -axis direction, it is appropriate to approximate the intermediate layer as aligned with x , as the orientation angle is unknown and small. Similarly, for the upper sublayer within the exocuticle, the fibers that compose this sublayer can be assumed to be oriented at 20° with respect to the x -axis.

The formal mathematical description of the laminate model, based on CLT [18] and the premises laid out above, is now described using a standard formulation [18, 28]. The global coordinate system (x, y and z) is defined in figure 5(a), where z is oriented in the direction normal to the tibia surface, thus perpendicular to the cuticular layers. The local coordinate system (1, 2 and 3), which corresponds to the principal (or natural) material directions of a lamina, is such that axis 1 coincides with the fibers direction, axis 2 is across fibers, and axis 3 is perpendicular to the lamina plane. In the case of a Bouligand, the 1-axis is the direction of the fibers in its midplane lamina (x -axis). The local coordinate system is used to calculate the lamina and Bouligand layer elastic constants (table S1), which, after angular transformation to the global coordinate system, allow calculation of the overall cuticle laminate elastic constants (table S2 and figure 6).

When the tibia laminate is under load (figure 5(a)), the in-plane forces N_x and N_y and in-plane shear force N_{xy} , along with the bending moments M_x and M_y and torsional moment M_{xy} , per unit laminate length, can be related to the normal and shear strains ε_x^0 , ε_y^0 and γ_{xy}^0 at the laminate midplane, and curvatures κ_x , κ_y and κ_{xy} , according



to the following relation:

$$\begin{bmatrix} \mathbf{N} \\ \mathbf{M} \end{bmatrix} = \begin{bmatrix} \mathbf{A} & \mathbf{B} \\ \mathbf{B} & \mathbf{D} \end{bmatrix} \begin{bmatrix} \boldsymbol{\varepsilon}^0 \\ \boldsymbol{\kappa} \end{bmatrix}, \quad (4)$$

where \mathbf{N} , \mathbf{M} , $\boldsymbol{\varepsilon}^0$ and $\boldsymbol{\kappa}$ are vectors containing components in the x, y (tensile) and xy (shear) directions. The 6×6 laminate stiffness matrix contains four 3×3 stiffness matrices: \mathbf{A} (laminate extensional stiffness), \mathbf{B} (laminate coupling stiffness), and \mathbf{D} (laminate bending stiffness) [18], given by:

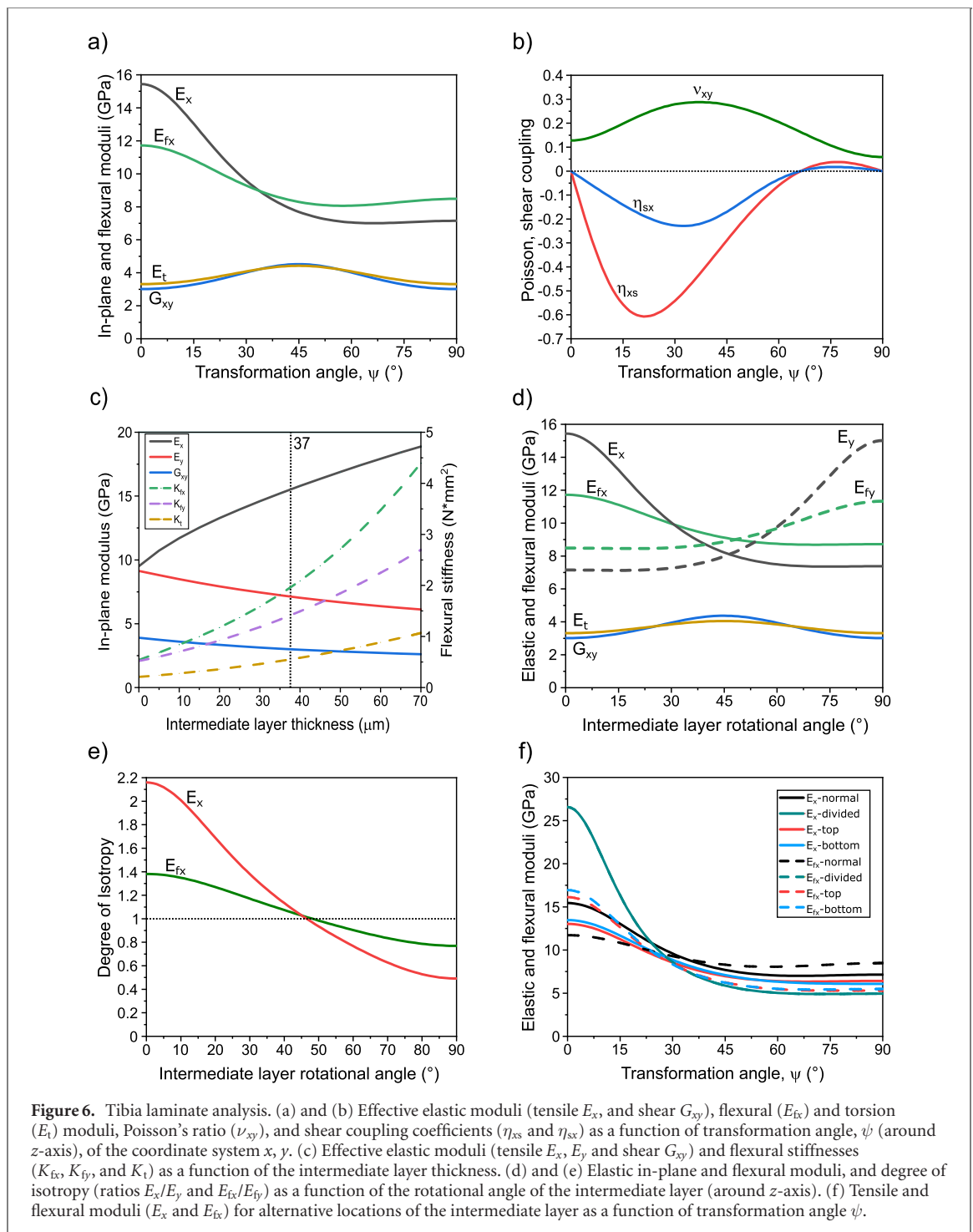
$$\begin{aligned} \mathbf{A} &= \int_{-t/2}^{t/2} \bar{\mathbf{Q}}_k dz \\ \mathbf{B} &= \int_{-t/2}^{t/2} \bar{\mathbf{Q}}_k z dz \\ \mathbf{D} &= \int_{-t/2}^{t/2} \bar{\mathbf{Q}}_k z^2 dz, \end{aligned} \quad (5)$$

where t is the thickness of the laminate, z is the distance from the middle surface of the laminate (midplane), and $\bar{\mathbf{Q}}_k$ is the 3×3 stiffness matrix of lamina k at position z , transformed from the lamina material (local) coordinates to the laminate global coordinates. Because of the asymmetric imbalanced nature of the tibia laminate structure, coupling effects within the structure are expected to arise under external stress, resulting in $\mathbf{B} \neq 0$.

3.5. Shear interlocking and interconnections

The usefulness of such a model as described above, when applied to a biological tissue with all its intricacies and variability of basic material properties, is less in its ability to accurately predict the mechanical performance, than in its ability to identify the trends of the structural behavior. For example, we expect the model to answer questions such as how is the structure optimized between the contradicting requirements for strength, stiffness and toughness, or what is the contribution of an intermediate layer to the overall mechanical performance. Keeping that goal in mind, to achieve a reliable representation of the actual structure, the model was calibrated to the experimental results.

The tibia exoskeleton consists of laminae of proteinaceous matrix reinforced by chitin fibers. The data on the mechanical properties of these elementary material components is known to vary over a wide range [29]. Thus, model calibration assists in tuning the protein and chitin properties, within the ranges found in the literature, to obtain laminate elastic properties that match the magnitudes measured in the bending tests. This being performed, it was found that the shear stiffness of the modeled cuticle laminate leads not only to anisotropic laminate stiffness, but also to lower stiffness values compared to the nearly isotropic properties measured in the bending test. To resolve this inconsistency, the mechanical effect of two



important structural features observed in the cuticle structure was examined (figures 5(a) and S6), and incorporated in the modelling inputs: (i) interlocking surfaces between Bouligand units, and (ii) interconnections between chitin fibers. These features are now described in more detail, as their implication goes beyond the specific modeling in the current study toward a more general approach for modeling such biological tissues and toward new types of synthetic composites.

The interlocking and interconnecting structural features reflect a fundamental difference between a biological laminate and current engineering

laminates, as synthetic laminates typically consist of wide laminae that are not segmented into multiple separate units such as Bouligands (BLUs). Furthermore, fibers in synthetic laminae are embedded individually and independently within the matrix, whereas in a biological lamina they also have direct fibrous interconnections between each other. In synthetic laminates, the in-plane shear modulus is typically relatively low, because it is dominated by the matrix modulus which is very low compared to that of the fibers, whereas in the tibia cuticle this deficiency is overcome by both interlocking and interconnecting.

The shear interlocking mechanism between BLUs was described by Greenfeld *et al* [16], where the BLUs can nest into each other, as a result of an off-axis twisting architecture (figure S6(a)). The BLU is thus a warped asymmetric helicoid, whose interface with neighboring BLUs is three-dimensional, much like a 3D jigsaw puzzle. When in-plane shear is applied to a BLU layer, some of the shear stress is converted to compression between BLUs, thereby increasing the effective shear stiffness of the structure.

The shear interconnecting mechanism between fibers in a lamina is realized by chitin fibers which instead of running independently in the lamina plane, interconnect to adjacent chitin fibers, as illustrated in figure 5(a) and seen in figure S6(b) and previously described by Raabe *et al* [30] in the lobster cuticle. When in-plane shear is applied on such an interconnected lamina, some of the shear stress is borne as tension in the interconnecting fibers, resulting in effectively higher shear stiffness. To demonstrate this effect, imagine two neighboring fibers, cross-connected by two interconnecting fibers; when shear is applied, the two main fibers are displaced in opposite directions, transmitting tension to one of the interconnecting fibers; if the shear load is reversed, the second interconnecting fiber will sense tension. Such thin unidirectional laminae are basic building blocks throughout the cuticle, as the higher-level laminates consist of numerous such angle-plyed laminae placed one on top of the other. Therefore, this feature affects the whole laminate, including the Bouligands and the unidirectional layers.

Both mechanisms, interlocking surfaces between Bouligands and chitin fiber interconnections, resist displacement under in-plane and out-of-plane shear stresses, without affecting the other in-plane and out-of-plane tensile and flexural properties. Figure 5(b) depicts the flexural modulus of the tibia as a function of the transformation angle ψ with respect to the z -axis. When ignoring the fiber interconnections and BLU interlocking surfaces in the analysis, there is a significant gap between the model (dashed red curve) and the experimental results (green squares), where a deep minimum is seen in the model at $\sim 45^\circ$ orientation. A more suitable fitting of the model (solid blue curve) to the experimental results is obtained when considering higher shear properties at the lamina level as a result of fiber interconnections and, at the BLUs level, as a result of interlocking surfaces. In-depth theoretical and experimental analysis of these mechanisms is left for future research, and therefore the fit was achieved by tuning the shear stiffness of the protein at the lamina level and the shear stiffness of the BLU, augmented by fitting factors of 1.5 and 3, respectively, both incorporated in table S1, and reflected in the cuticle laminate properties.

Matrix stiffening is critical for structural stability, as demonstrated by our modeling, and nature adopts various strategies for matrix strengthening,

such as fibers interconnections in the SP tibia cuticle, ion metals in the spider fang [31], the inclusion of biominerals in crustaceans [4], and matrix sclerotization in insects [32, 33].

3.6. Laminate elastic properties

The elastic properties of the tibia laminate are calculated from the laminate compliance matrix, as acquiring these properties directly from the stiffness matrices leads to complex expressions; additionally, unlike the displacements, the applied loads are usually known [18]. The laminate 6×6 compliance matrix is obtained by inverting the stiffness matrix of equation (4):

$$\begin{bmatrix} \varepsilon^0 \\ \kappa \end{bmatrix} = \begin{bmatrix} \mathbf{a} & \mathbf{b} \\ \mathbf{c} & \mathbf{d} \end{bmatrix} \begin{bmatrix} \mathbf{N} \\ \mathbf{M} \end{bmatrix}. \quad (6)$$

To calculate the forces per unit laminate length under in-plane loading (no moments), the equation for average laminate stresses is used, $\bar{\sigma} = \mathbf{N}/H$, where H is the average height of the laminate, taken from the thickness measurements for each layer (using SEM): $H = 121 \mu\text{m}$. Thus, $\varepsilon^0 = \mathbf{a}\mathbf{N} = H\mathbf{a}\bar{\sigma}$, and the laminate effective engineering constants are obtained from the matrix \mathbf{a} by separately calculating the strains for each loading condition [18].

The resulting engineering properties of the laminate from the analysis include three elastic moduli, two Poisson's ratios, and four shear coupling coefficients, a total of nine engineering constants. Additionally, the three effective flexural moduli, which include two bending moduli (E_{fx} and E_{fy}) and a torsional modulus (E_t), together with the bending stiffnesses (K_{fx} and K_{fy}) are calculated. (Note that the subscript f is used to denote 'flexural' rather than 'fiber'.)

The elastic modulus of a crystalline α -chitin taken into account is about 80 GPa, whereas the elastic modulus of the protein matrix is 1.2 GPa, within the range suggested elsewhere based on simulations [29]. Resultant lamina and BLU constants adapted from [16] are shown in table S1, and these are the basic building blocks for the whole cuticle laminate; these constants are with respect to the material coordinate system (1, 2, and 3). The fibers and matrix components, and consequently the lamina and BLU properties, are just an estimate, as the components data is limited and dependent on diverse simulation conditions. Since the aim of the analysis is the understanding of the benefits that the intermediate layer can provide to both the scorpion cuticle and bioinspired systems, accurate material constants are not critical.

The resulting elastic constants for the exocuticle, intermediate layer, and endocuticle, are shown in table S2. The exo- and endocuticle clearly exhibit a nearly in-plane isotropic behavior as a result of the diverse assembled morphologies of the layers. The resulting elastic constants for the complete tibia cuticle laminate are presented in figure 6 and table S2. We

note that, although it is possible to run the CLT model using just the top data of the three major layers, and obtain similar general trends as when running with the fully detailed structure, the result is less accurate and information on local behavior such as critically stressed regions might be lost.

Distinctive values of the tensile moduli are observed in both x (E_x) and y (E_y) directions, where the former is significantly higher than the latter. Additionally, the flexural modulus in the x -direction (E_{fx}) (bending around y) is moderately higher than the one in the y -direction (E_{fy}) (bending around x). Both results indicate that the tibia laminate is nearly in-plane isotropic, and that it is much more isotropic than a single lamina or a unidirectional layer (e.g. the intermediate layer). Higher mechanical properties in the x -direction are indeed expected, as more fibers in the tibia are aligned with the x -orientation. Nevertheless, it can be appreciated that the assembly of diverse laminae, each strongly anisotropic, into a multiscale structure achieves nearly in-plane isotropy. The shear-normal cross-coupling constants (η_{ij}) demonstrate the structural stability of the tibia laminate under load.

These trends can be observed in figures 6(a) and (b), where the elastic constants are depicted as a function of the transformation angle ψ (around the z -axis) in the global coordinate system. Note that at $\psi = 90^\circ$ the properties in x are switched to y and vice versa. The shear (G_{xy}) and torsion (E_t) moduli have an evident peak seen at 45° . At intermediate values of ψ , substantial changes are noted in the η_{ij} values; a shear distortion in η_{xs} can be seen at loading angles approaching $\sim 20^\circ$, as a result of tension in the x -direction; the opposite coupling constant η_{sx} is less sensitive than η_{xs} . The coupling effect vanishes close to the principal axes x and y , yielding an uncoupled extensional behavior of the laminate. It has been suggested that the effect of η_{ij} relies on the shear strains of the matrix, which are higher at inclined angles [34]. Moreover, these matrix shear strains are also responsible for the Poisson's ratio (ν_{xy}) peak at intermediate values of ψ , as large matrix shear strains can induce not only shear distortions within the laminate, but also lateral contractions. Indeed, the model shows that the introduction of the fiber interconnections mechanism by increasing the protein shear stiffness, as described in the previous section, not only improves the isotropy (figure 5(b)) but also reduces the peaks of both the Poisson's ratio and shear-coupling constants.

3.7. Effect of the intermediate layer on elastic properties

The existence and role of an intermediate layer in the SP is a major research question in the current study, as this layer does not exist in other arthropods with claws. The intermediate layer has a noticeable effect on the tibia mechanical properties, as previously

discussed in the experimental section (figures 3(e) and S4). Here, we used the CLT model to better understand the effect of the intermediate layer on the overall cuticle laminate elastic properties. This was achieved by separately modulating the intermediate layer thickness, fibers direction, and location in the laminate, producing the laminate dependency on the intermediate layer. The modulation ranges went beyond the ranges found in the actual biological tissue, zero to double the layer thickness (figure 6(c)), 0° – 90° fibers rotation within the intermediate layer (figures 6(d) and (e)), and top/bottom/split locations (figure 6(f)).

The bending and torsion stiffnesses (K_{fx} , K_{fy} , and K_t) are significantly affected by the intermediate layer thickness as seen in figure 6(c). As the intermediate layer thickness is increased, the flexural stiffnesses increase regardless of the fibers orientation, due to the increase in the second moment of inertia of the cuticle ($I = bh^3/12$, where h is the intermediate layer thickness). This allows the cuticle to support higher flexural loads, at a small expense in the in-plane moduli E_y and G_{xy} . Both E_x and K_{fx} exhibit the steepest rise with cuticle thickness (figure 6(c)) because of the fiber orientation within the intermediate layer, which is predominantly in the x -direction.

Rotating the fibers within the intermediate layer (around the z -axis) has a critical impact on the elastic and flexural moduli of the cuticle and on its isotropic behavior (figures 6(d) and (e)). The intermediate layer is made of unidirectional fibers that will lead to higher mechanical properties in the orientation direction, as seen by the high values of E_x at 0° and E_y at 90° , for example. The optimal degree of isotropy in the tensile and flexural moduli would be achieved when the fibers orientation in the intermediate layer is close to 45° (value of 1 in figure 6(e)). However, this does not seem to be the orientation in the actual cuticle, possibly because at that orientation both the x and y values are close to the lowest apparent values, whereas at the actual 0° orientation the x value is high while the y value is moderately degraded.

The flexural modulus exhibits a higher degree of isotropy (values closer to 1) than the tensile modulus for any intermediate layer rotation angle (figure 6(e)), reaffirming that the tibia cuticle is a structure optimized to resist higher bending loads at the expense of lower tensile loads. Bearing in mind the biomechanical functionality of the tibia, which requires withstanding external bending loads due to localized pressure on the surface, the evolution of the SP has resulted in a tibia shielding structure fit for defense against predators. This was achieved by growing the tibia thickness through incorporation of an anisotropic intermediate layer, which increases the bending stiffness with only a small sacrifice in the in-plane stiffness of the cuticle (figure 6(c)).

This proposed mechanical hypothesis seems appropriate, considering that scorpions with a large chela usually are armed with weaker venom in their

stingers to defend against predators, so possibly their chela was mechanically optimized to meet the scorpion necessities [1]. For the scorpion to retain a certain flexural degree of isotropy, evolution has found it fit to integrate such an anisotropic layer in between the exo- and the endocuticle (both in-plane isotropic) rather than below, beneath or in both places at the same time (figure 6(f)). We see that the actual location of the intermediate layer (black solid and dashed curves) provides optimal isotropy compared to the three other locations.

3.8. Laminate strength modeling

In the case of a complex structure such as the tibia exoskeleton, it is challenging to evaluate the tensile and interlaminar stresses, as the exoskeleton morphology is hierarchical and varies with depth. The stresses are not only different in each layer, but also different with respect to the bending directions, whether in the xz or yz planes. As in the CLT elastic analysis, we assume that each lamina within the structure is in a state of plane stress in the xy -plane, therefore, the stresses in the z -direction can be neglected. Although in three-point bending there is a constant vertical shear stress, it can be neglected in beams with an aspect ratio (span/thickness) larger than 15, a condition satisfied here.

Two possible failure modes of the tibia exoskeleton were explored: (i) First Ply Failure (FPF), which occurs when the in-plane tensile stress exceeds the strength of a lamina, causing the lamina to break; and (ii) interlaminar failure (ILF), which occurs when the in-plane shear stress exceeds the strength of the matrix between two adjacent laminae, causing delamination. In the following analysis, we apply these two criteria, to assess the failure mechanism that the tibia experiences under an external load [28]. Among other things, we are specifically interested in the effect of the intermediate layer on the strength, taking into account not only the forces applied during the three-point bending measurements but also the inputs used for the laminate analysis.

Consider the free body diagram of the tibia structure in figure 7(a), which shows bending in the zx -plane. The following description and equations also apply to bending in the zy -plane by substituting x by y . The beam is of width w and span length $2L$, and is loaded at three points by a force (per unit width) $-2F$ at the center and F at each support. The bending moment at position x along the beam is $M_x = Fx/w$ per unit laminate width, and the maximum moment value is at the beam center, $M_{\max} = FL/w$.

The strain at any point in a laminate under load is related to the laminate plane strains and curvatures by $\varepsilon = \varepsilon^0 + z\kappa$, where z is the distance from the laminate midplane [28]. The corresponding in-plane stresses are $\sigma = \bar{Q}_k \varepsilon$, where \bar{Q}_k is lamina k stiffness matrix transformed into the laminate global xyz system. Using equation (6) for a flexural moment

M_x (no in-plane loads, $\mathbf{N} = 0$), the tensile stress in the x -direction is given by [28]:

$$\sigma_x = [\bar{Q}_k(\mathbf{b} + z\mathbf{d})]_{xx} M_x, \quad (7)$$

where \mathbf{b} and \mathbf{d} are the compliance matrices of the laminate (see equation (6)), and the subscript xx denotes element 11 in the matrix in brackets (element 22 for bending in y). The selection of the lamina index k is such that the position z lays in the lamina. Note that because the tibia laminate is asymmetric and imbalanced, the compliance matrix $\mathbf{b} \neq 0$. The moment M_x depends on the position along the beam and on the sample direction, such that at the beam center $M_x = M_{\max}$.

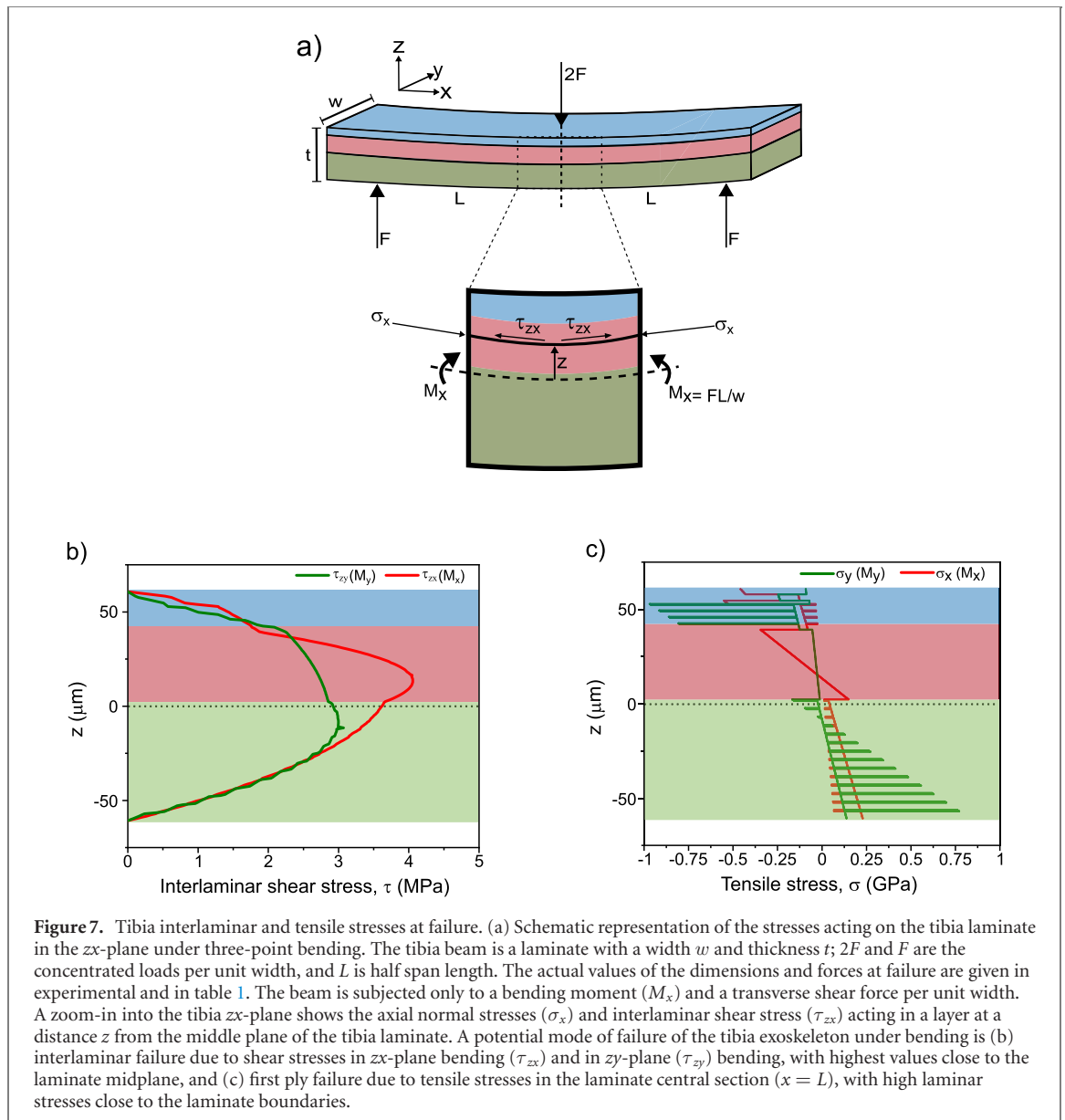
The shear stress τ_{zx} at a position z in the laminate exerts a force $\tau_{zx} dx$ (per unit width) on a segment of length dx (figure 7(a)). The difference in the tensile stress across the segment in the x -direction, $d\sigma_x$, generates a balancing force $d\sigma_x dz$ (per unit width) on a segment of height dz . Integrating over the full height of the segment, from z to $t/2$, and equating to the shear force, the resulting shear stress is given by [28]:

$$\tau_{zx} = \int_z^{t/2} \frac{d\sigma_x}{dx} dz' = V_z \int_z^{t/2} [\bar{Q}_k(\mathbf{b} + z'\mathbf{d})]_{xx} dz', \quad (8)$$

where V_z is the constant shear force, $V_z = dM_x/dx = F/w$, per unit laminate width. Note that the matrix in brackets is independent of x , and therefore not differentiated, and that the resulting shear stress at a constant height z is constant throughout the laminate. To obtain the interlaminar shear stress between lamina k and lamina $k + 1$, substitute $z = z_k$ where z_k is the top position of lamina k .

The interlaminar shear stress (at failure) over the tibia thickness is shown in figure 7(b). The shear stress distribution is almost symmetric around the middle plane: it disappears at the free surfaces ($z \sim \pm 60 \mu\text{m}$), while achieving a maximum value near the center of the intermediate layer when bending in the zx -plane, and at the upper layers of the endocuticle when bending in the zy -plane. These results aid as a guide in understanding the shear transfer mechanism between two layers in the tibia exoskeleton.

Figure 7(b) suggests that the shear strength at the interlaminar protein matrix is between 3 and 4 MPa, the maximum failure stresses when bending in the zy and zx planes, respectively. The difference in the interlaminar strengths with respect to sample direction may possibly reflect the effect of fibers interconnections, discussed above, on the protein matrix effective shear strength. As mentioned earlier, since the majority of fibers are oriented in the x -direction, the interlaminar strength in that direction could be more predominant. Alternatively, it is possible that the molecular orientation of the protein macromolecules in the tightly-sandwiched interlaminar matrix is affected by the neighboring chitin fibers, resulting in co-aligning that enhances the matrix



strength in the fibers direction. Hence, the interlaminar proteinaceous matrix is not isotropic, because its strength most probably depends on the direction of the fibers in the adjacent laminae on both sides. This finding is of high general importance, as the interlaminar strength is an unknown material property which to our knowledge was not measured directly in a biological tissue.

The interlaminar shear stresses at the intermediate layer, when bending in the zx -plane, reach a maximum slightly below the intermediate layer center (figure 7(b)), suggesting that laminae separation in the 0° samples should take place within the intermediate layer. Such behavior was indeed observed in our experimental results (figure 4(c)). When bending in the zy -plane, the maximal interlaminar stress in the intermediate layer moves towards the upper part of the endocuticle, and delamination is expected between an interlayer and a BLUs layer or inside a BLU. The interlaminar stress profile is less steep in zy

bending compared to zx bending, because the stress is carried in the weakest direction of the intermediate layer (the y -direction, across the fibers), compared to the fibers direction in zx bending. The maximum interlaminar shear stress in the zy -plane is experienced in the endocuticle due to the gap in the elastic moduli and Poisson ratios between the interlayer and Bouligand units as seen in table S2 and discussed by Tahani *et al* [35].

Pipes and Pagano [36] discussed the effect of fiber orientation on the interlaminar shear stresses in unidirectional laminated composites, showing that the maximum τ_{zx} occurs in a 35° direction. For the sake of simplicity, in the current work the intermediate layer was considered to be oriented with the x -axis, but figure 1(e) and S1(b) show that the intermediate layer displays a small degree of orientation with respect to x . However, modulating the transformation angle ψ or the intermediate layer rotation angle in the model did not yield higher interlaminar stresses

in the intermediate layer, compared to the zx bending case. Whitney and Browning [37] observed that the delamination process in fiber-reinforced composites under three-point bending usually takes place after the appearance of a vertical crack; this peculiarity was not observed in the tibia cuticle.

The distribution of the tensile stresses σ_x and σ_y (at failure) through the tibia thickness as a result of bending moments M_x and M_y , respectively, is depicted in figure 7(c). It can be seen that the tibia morphology can change the magnitude of the stresses in both the compression region above the middle plane ($z = 0$) and the tension region beneath the middle plane. As expected, the outer layers experience higher bending stresses as they are far away from the middle plane, seen in the exo- and endocuticle where the stress profile is increasing towards the laminate boundary. The maximum stress levels in the zy -bending case, which occur in the interlayers (the sharp peaks in figure 7(c)), are significantly higher than in the zx -bending, likely because the interlayers are unidirectional in the y -direction. Thus, if FPF occurs, it would most probably happen at one of the outbound interlayers. Figure 7(c) suggests that the tensile strength of a unidirectional lamina should be above about 1 MPa, the maximum failure stress when bending in the zy plane.

The presence of high values of laminar stresses (σ_x and σ_y) and shear stresses (τ_{zx} and τ_{zy}), which may cause lamina fracture or interlaminar delamination, respectively, is greatly affected by fiber orientation and volume fraction, as reported for synthetic composites [38] and seen in our analysis. Although the failure mechanisms cannot be foreseen using classical laminate analysis, as the materials actual strength properties are not available, putting together the experiments and modeling we may point at delamination as the predominant failure mechanism in the cuticle. Nature provides an approach that can aid in resisting failure in synthetic composites under external stress, namely the application of hierarchical structures and varying morphology. A prominent example in the tibia cuticle is the integration of the thin unidirectional interlayers oriented along the y -axis, which functions to balance the Bouligands' x -direction preference, achieving an in-plane isotropic behavior at the cuticle laminate level. Such an approach may be considered when designing a bioinspired laminate.

4. Conclusions

Structural analysis of the tibia exoskeleton of the SP reveals the existence of an intermediate layer of vertically arranged lamellae of unidirectional fibers, comprising about 30% of the total cuticle thickness. The presence of this layer is unique as it does not exist in the scorpion body cuticle, nor in other broadly studied arthropods having claws such as lobsters or crabs.

The intermediate layer increases the local thickness of the cuticle, impacting the mechanical properties of the tibia structure.

A combined experimental and theoretical analysis was applied to investigate the effect of the cuticle microstructure on the tibia macro-mechanical properties. Bending tests of tibia samples in dry and wet conditions show a balanced structural stiffness, strength and work to fracture, properties which are typically difficult to achieve simultaneously. Additionally, the bending tests show that hydration conditions have a significant impact on the mechanisms of energy absorption during failure: a dry cuticle absorbs significant amounts of energy through the elastic region, resulting in local delamination or laminae failure, whereas a wet cuticle uses plastic deformation to absorb energy through damage tolerance and damage diffusion. It is thought-provoking that these macro-level properties are the result of a complex multilevel structure rather than intrinsic material properties.

The cuticle laminated microstructure, consisting of 42 sublayers arranged in 8 hierarchical levels, was modeled by classical laminate analysis, resulting in good agreement with the experimental results. The effects of Bouligand units interlocking, as well as chitin fibers interconnections within the cuticle, were integrated into the model. By considering the morphology and fiber orientation at each layer, which is basically an anisotropic building block, the analytical model demonstrates the influence of hierarchical structures on the isotropic behavior found in the tibia exoskeleton. The model allows estimation of the interlaminar protein shear strength, 3–4 MPa, previously not measured.

In terms of the *in vivo* mechanical functionality, the scorpion has evolved a practical solution which resists high contact loads when defending against a predator, taking advantage of its large-sized tibia used as a shield and the simultaneously enhanced flexural stiffness and energy absorption. The integration of the anisotropic intermediate layer between two quasi-isotropic layers teaches us a suitable method to assure mechanical in-plane balance, evidently beneficial for the survivability of the *Scorpio Palmatus*.

The structural strategies found in nature are very different from those applied in synthetic designs, as biological materials are much weaker and their construction is by means of self-assembly. However, inspiration may be derived from the structural approach implemented in the cuticle, which evolved to achieve balanced strength, stiffness, toughness, and isotropy. We allude to several cuticle-inspired biomimetics ideas: (1) damage tolerance and diffusion may be expanded by multilevel hierarchical structure; (2) bending stiffness may be increased by adding an intermediate anisotropic layer; (3) shear stiffness and strength may be improved by mechanical interlocking between repeating subunits; and, (4)

stiffness and strength of soft matrix may be enhanced by interconnections between reinforcing fibers.

Further research is expected to solidify these findings, to address: (i) the capability of the scorpion tibia to resist impact loads through fracture toughness, allowing a suitable comparison of the tibia resistance to fracture in other arthropods; (ii) the scale-dependent toughening mechanisms by *in-situ* characterization; (iii) the mechanisms of fibers interconnections and Bouligand surface interlocking; and (iv) similar studies in other species of scorpions with diverse chela size and shape.

Author contributions

IK and IG contributed equally to this work. IK conceived the idea, captured the scorpions, designed and carried out the experiments, performed the theoretical CLT analysis, and wrote and edited the manuscript. IG contributed to the CLT analytical model, and to editioning and revisioning the manuscript. HDW coordinated the study and edited the manuscript. All authors discussed the results and interpretations and reviewed the manuscript.

Ethical disclosure

The Israeli law 'Animal suffering (experiments on animals), 1994' excludes invertebrate animals (including scorpions), and therefore no formal ethical approval was required to conduct the experiments.

Acknowledgments

We gratefully acknowledge the help provided in collecting the scorpions species by Yoram Zvik from Hoopoe, Yeruham's Ornithology and Ecology Center and Ohad Yalomi from the Israel Nature and Parks Authorities. Special thanks to Dr Sidney R Cohen and Dr Irit Goldian for their help with the AFM measurements, and to Dr Nili Dezorella for assistance with the TEM experiments. The authors would like to acknowledge partial support from the GMJ Schmidt Minerva Centre of Supramolecular Architectures at the Weizmann Institute. This research was also made possible in part by the generosity of the Harold Perlman family. H Daniel Wagner is the recipient of the Livio Norzi Professorial Chair in Materials Science.

ORCID iDs

Israel Kellersztein  <https://orcid.org/0000-0002-8838-818X>

Israel Greenfeld  <https://orcid.org/0000-0001-9683-7267>

H Daniel Wagner  <https://orcid.org/0000-0002-0741-2169>

References

- [1] van der Meijden A, Herrel A and Summers A 2010 Comparison of chela size and pincer force in scorpions; getting a first grip *J. Zool.* **280** 319–25
- [2] Polis G A 1990 *The Biology of Scorpions* (California: Stanford University Press)
- [3] Weaver J C *et al* 2012 The stomatopod dactyl club: a formidable damage-tolerant biological hammer *Science* **336** 1275–80
- [4] Cheng L, Wang L and Karlsson A M 2008 Image analyses of two crustacean exoskeletons and implications of the exoskeletal microstructure on the mechanical behavior *J. Mater. Res.* **23** 2854–72
- [5] Raabe D, Sachs C and Romano P 2005 The crustacean exoskeleton as an example of a structurally and mechanically graded biological nanocomposite material *Acta Mater.* **53** 4281–92
- [6] Cribb B W, Rathmell A, Charters R, Rasch R, Huang H and Tibbetts I R 2009 Structure, composition and properties of naturally occurring non-calcified crustacean cuticle *Arthropod Struct. Dev.* **38** 173–8
- [7] Krishnan G 1953 On the cuticle of the scorpion *Palamneus Swammerdami* Q. *J. Microsc. Sci.* **94** 11–21 <https://jcs.biologists.org/content/s3-95/31/371.short>
- [8] Krishnan G 1954 The epicuticle of an arachnid, *Palamneus* Q. *J. Microsc. Sci.* **95** 371–81 <https://jcs.biologists.org/content/s3-95/31/371.short>
- [9] Dennell R 1975 The structure of the cuticle of the scorpion *pandinus imperator* (Koch) *Zool. J. Linn. Soc.* **56** 249–54
- [10] Mutvei H 1974 SEM studies on arthropod exoskeletons. Part I: Decapod crustaceans, *Homarus gammarus* (L) and *Carcinus maenas* (L) Vol 4 *Bull. Geol. Institutions Univ. Uppsala* (Sweden: DA) pp 73–80
- [11] van der Meijden A, Kleinteich T and Coelho P 2012 Packing a pinch: functional implications of chela shapes in scorpions using finite element analysis *J. Anat.* **220** 423–34
- [12] Van Der Meijden A, Coelho P L, Sousa P and Herrel A 2013 Choose your weapon: defensive behavior is associated with morphology and performance in scorpions *PLoS One* **8** e78955
- [13] Kellersztein I, Cohen S R, Bar-On B and Wagner H D 2019 The exoskeleton of scorpions pincers: structure and micro-mechanical properties *Acta Biomater.* **94** 565–73
- [14] Hadley N F and Jackson L L 1977 Chemical composition of the epicuticular lipids of the scorpion, *paruroctonus mesaensis* *Insect Biochem.* **7** 85–9
- [15] Toolson E C and Hadley N F 1977 Cuticular permeability and epicuticular lipid composition in two Arizona Vejovid scorpions *Physiol. Zool.* **50** 323–30
- [16] Greenfeld I, Kellersztein I and Wagner H D 2020 Nested helicoids in biological microstructures *Nat. Commun.* **11** 1–12
- [17] Sierakowski R L and Newaz G M 1995 *Damage Tolerance in Advanced Composites* (Pennsylvania: Technomic Publishing Company)
- [18] Gibson R F 1994 *Principles of Composite Material Mechanics* 3rd edn (Boca Raton, FL: CRC Press)
- [19] Klocke D and Schmitz H 2011 Water as a major modulator of the mechanical properties of insect cuticle *Acta Biomater.* **7** 2935–42
- [20] Aberle B, Jemmali R and Dirks J-H 2017 Effect of sample treatment on biomechanical properties of insect cuticle *Arthropod Struct. Dev.* **46** 138–46
- [21] Lokes R S 1993 Materials with structural hierarchy *Nature* **361** 511–5
- [22] Chu X X, Wu Z X, Huang R J, Zhou Y and Li L F 2010 Mechanical and thermal expansion properties of glass fibers reinforced PEEK composites at cryogenic temperatures *Cryogenics* **50** 84–8
- [23] Yilmaz T and Sinmazcelik T 2010 Effects of hydrothermal aging on glass-fiber/polyetherimide (PEI) composites *J. Mater. Sci.* **45** 399–404

- [24] Dirks J-H and Taylor D 2012 Fracture toughness of locust cuticle *J. Exp. Biol.* **215** 1502–8
- [25] Spearing S M and Evans A G 1992 The role of fiber bridging in the delamination resistance of fiber-reinforced composites *Acta Metall. Mater.* **40** 2191–9
- [26] Filshie B K and Hadley N F 1979 Fine structure of the cuticle of the desert scorpion, *Hadrurus arizonensis* *Tissue Cell* **11** 249–62
- [27] Abisset E, Daghia F and Ladevèze P 2011 On the validation of a damage mesomodel for laminated composites by means of open-hole tensile tests on quasi-isotropic laminates *Composites A* **42** 1515–24
- [28] Daniel I M and Ishai O 2006 *Engineering Mechanics of Composite Materials* (Oxford: Oxford University Press)
- [29] Politi Y, Bar-On B and Fabritius H O 2019 Mechanics of arthropod cuticle-versatility by structural and compositional variation *Architected Materials in Nature and Engineering* (Berlin: Springer) pp 287–327
- [30] Raabe D, Romano P, Sachs C, Fabritius H, Al-Sawalmih A, Yi S-B, Servos G and Hartwig H G 2006 Microstructure and crystallographic texture of the chitin–protein network in the biological composite material of the exoskeleton of the lobster *Homarus americanus* *Mater. Sci. Eng. A* **421** 143–53
- [31] Degtyar E, Harrington M J, Politi Y and Fratzl P 2014 The mechanical role of metal ions in biogenic protein-based materials *Angew. Chem., Int. Ed.* **53** 12026–44
- [32] Wang L-Y, Jafarpour M, Lin C-P, Appel E, Gorb S N and Rajabi H 2019 Endocuticle sclerotisation increases the mechanical stability of cuticle *Soft Matter* **15** 8272–8
- [33] Wang L Y, Rajabi H, Ghoroubi N, Lin C P and Gorb S N 2018 Biomechanical strategies underlying the robust body armour of an aposematic weevil *Front. Physiol.* **9** 1410
- [34] Hull D and Clyne T W 1996 *An Introduction to Composite Materials* 2nd edn (Cambridge: Cambridge University Press)
- [35] Tahani M and Nosier A 2004 Accurate determination of interlaminar stresses in general cross-ply laminates *Mech. Adv. Mater. Struct.* **11** 67–92
- [36] Pipes R B and Pagano N J 1970 Interlaminar stresses in composite laminates under uniform axial extension *J. Compos. Mater.* **4** 538–48
- [37] Whitney J M and Browning C E 1985 On short-beam shear tests for composite materials *Exp. Mech.* **25** 294–300
- [38] Wang Y, Li J and Do P B 1995 Properties of composite laminates reinforced with E-glass multiaxial non-crimp fabrics *J. Compos. Mater.* **29** 2317–33